LETTER

The Cancer Cell Line Encyclopedia enables predictive modelling of anticancer drug sensitivity

Jordi Barretina[1,2,3]†*, Giordano Caponigro[4]*, Nicolas Stransky[1]*, Kavitha Venkatesan[4]*, Adam A. Margolin[1]†*, Sungjoon Kim[5], Christopher J. Wilson[4], Joseph Lehár[4], Gregory V. Kryukov[1], Dmitriy Sonkin[4], Anupama Reddy[4], Manway Liu[4], Lauren Murray[1], Michael F. Berger[1]†, John E. Monahan[4], Paula Morais[1], Jodi Meltzer[4], Adam Korejwa[1], Judit Jané-Valbuena[1,2], Felipa A. Mapa[4], Joseph Thibault[5], Eva Bric-Furlong[4], Pichai Raman[4], Aaron Shipway[5], Ingo H. Engels[5], Jill Cheng[6], Guoying K. Yu[6], Jianjun Yu[6], Peter Aspesi Jr[4], Melanie de Silva[4], Kalpana Jagtap[4], Michael D. Jones[4], Li Wang[4], Charles Hatton[3], Emanuele Palescandolo[3], Supriya Gupta[1], Scott Mahan[1], Carrie Sougnez[1], Robert C. Onofrio[1], Ted Liefeld[1], Laura MacConaill[3], Wendy Winckler[1], Michael Reich[1], Nanxin Li[5], Jill P. Mesirov[1], Stacey B. Gabriel[1], Gad Getz[1], Kristin Ardlie[1], Vivien Chan[6], Vic E. Myer[4], Barbara L. Weber[4], Jeff Porter[4], Markus Warmuth[4], Peter Finan[4], Jennifer L. Harris[5], Matthew Meyerson[1,2,3], Todd R. Golub[1,3,7,8], Michael P. Morrissey[4]*, William R. Sellers[4]*, Robert Schlegel[4]* & Levi A. Garraway[1,2,3]*

The systematic translation of cancer genomic data into knowledge of tumour biology and therapeutic possibilities remains challenging. Such efforts should be greatly aided by robust preclinical model systems that reflect the genomic diversity of human cancers and for which detailed genetic and pharmacological annotation is available[1]. Here we describe the Cancer Cell Line Encyclopedia (CCLE): a compilation of gene expression, chromosomal copy number and massively parallel sequencing data from 947 human cancer cell lines. When coupled with pharmacological profiles for 24 anticancer drugs across 479 of the cell lines, this collection allowed identification of genetic, lineage, and gene-expression-based predictors of drug sensitivity. In addition to known predictors, we found that plasma cell lineage correlated with sensitivity to IGF1 receptor inhibitors; _AHR_ expression was associated with MEK inhibitor efficacy in _NRAS_-mutant lines; and _SLFN11_ expression predicted sensitivity to topoisomerase inhibitors. Together, our results indicate that large, annotated cell-line collections may help to enable preclinical stratification schemata for anticancer agents. The generation of genetic predictions of drug response in the preclinical setting and their incorporation into cancer clinical trial design could speed the emergence of 'personalized' therapeutic regimens[2].

Human cancer cell lines represent a mainstay of tumour biology and drug discovery through facile experimental manipulation, global and detailed mechanistic studies, and various high-throughput applications. Numerous studies have used cell-line panels annotated with both genetic and pharmacological data, either within a tumour lineage[3–5] or across multiple cancer types[6–12]. Although affirming the promise of systematic cell line studies, many previous efforts were limited in their depth of genetic characterization and pharmacological interrogation.

To address these challenges, we generated a large-scale genomic data set for 947 human cancer cell lines, together with pharmacological profiling of 24 compounds across ~500 of these lines. The resulting collection, which we termed the Cancer Cell Line Encyclopedia (CCLE), encompasses 36 tumour types (Fig. 1a and Supplementary Table 1; see also http://www.broadinstitute.org/ccle). All cell lines were characterized by several genomic technology platforms. The mutational status of >1,600 genes was determined by targeted massively parallel sequencing, followed by removal of variants likely to be germline events (Supplementary Methods). Moreover, 392 recurrent mutations affecting 33 known cancer genes were assessed by mass spectrometric genotyping[13] (Supplementary Table 2 and Supplementary Fig. 1). DNA copy number was measured using high-density single nucleotide polymorphism arrays (Affymetrix SNP 6.0; Supplementary Methods). Finally, messenger RNA expression levels were obtained for each of the lines using Affymetrix U133 plus 2.0 arrays. These data were also used to confirm cell line identities (Supplementary Methods and Supplementary Figs 2–4).

We next measured the genomic similarities by lineage between CCLE lines and primary tumours from Tumorscape[14], expO, MILE and COSMIC data sets (Fig. 1b–d and Supplementary Methods). For most lineages, a strong positive correlation was observed in both chromosomal copy number and gene expression patterns (median correlation coefficients of 0.77, range = 0.52–0.94, $P < 10^{-15}$, for copy number, and 0.60, range = 0.29–0.77, $P < 10^{-15}$, for expression, respectively; Fig. 1b, c and Supplementary Tables 3 and 4), as has been described previously[3–5,15]. A positive correlation was also observed for point mutation frequencies (median correlation coefficient = 0.71, range = −0.06–0.97, $P < 10^{-2}$ for all but 3 lineages; Supplementary Fig. 5), even when _TP53_ was removed from the data set (median correlation coefficient = 0.64, range = −0.31–0.97, $P < 10^{-2}$ for all but 3 lineages; Fig. 1d and Supplementary Table 5). Thus, with relatively few exceptions (Supplementary Information), the CCLE may provide representative genetic proxies for primary tumours in many cancer types.

Given the pressing clinical need for robust molecular correlates of anticancer drug response, we incorporated a systematic framework to ascertain molecular correlates of pharmacological sensitivity _in vitro_. First, 8-point dose–response curves for 24 compounds (targeted and cytotoxic agents) across 479 cell lines were generated (Supplementary Tables 1 and 6, and Supplementary Methods). These curves were represented by a logistical sigmoidal function with a maximal effect level (A_{max}), the concentration at half-maximal activity of the compound (EC_{50}), a Hill coefficient representing the sigmoidal transition, and the concentration at which the drug response reached an absolute inhibition of 50% (IC_{50}).

Broadly active compounds, exemplified by the HDAC inhibitor LBH589 (panobinostat), showed a roughly even distribution of A_{max} and EC_{50} values across most cell lines (Fig. 2a). In contrast, the RAF inhibitor PLX4720 had a more selective profile: A_{max} or EC_{50} values for most cell lines could be categorized as 'sensitive' or 'insensitive' to

[1]The Broad Institute of Harvard and MIT, Cambridge, Massachusetts 02142, USA. [2]Department of Medical Oncology, Dana-Farber Cancer Institute, Harvard Medical School, Boston, Massachusetts 02115, USA. [3]Center for Cancer Genome Discovery, Dana-Farber Cancer Institute, Harvard Medical School, Boston, Massachusetts 02115, USA. [4]Novartis Institutes for Biomedical Research, Cambridge, Massachusetts 02139, USA. [5]Genomics Institute of the Novartis Research Foundation, San Diego, California 92121, USA. [6]Novartis Institutes for Biomedical Research, Emeryville, California 94608, USA. [7]Department of Pediatric Oncology, Dana-Farber Cancer Institute, Boston, Massachusetts 02115, USA. [8]Howard Hughes Medical Institute, Chevy Chase, Maryland 20815, USA. †Present addresses: Novartis Institutes for Biomedical Research, Cambridge, Massachusetts 02139, USA (J.B.); Sage Bionetworks, 1100 Fairview Ave. N., Seattle, Washington 98109, USA (A.A.M.); Department of Pathology, Memorial Sloan-Kettering Cancer Center, New York, New York 10065, USA (M.F.B.).
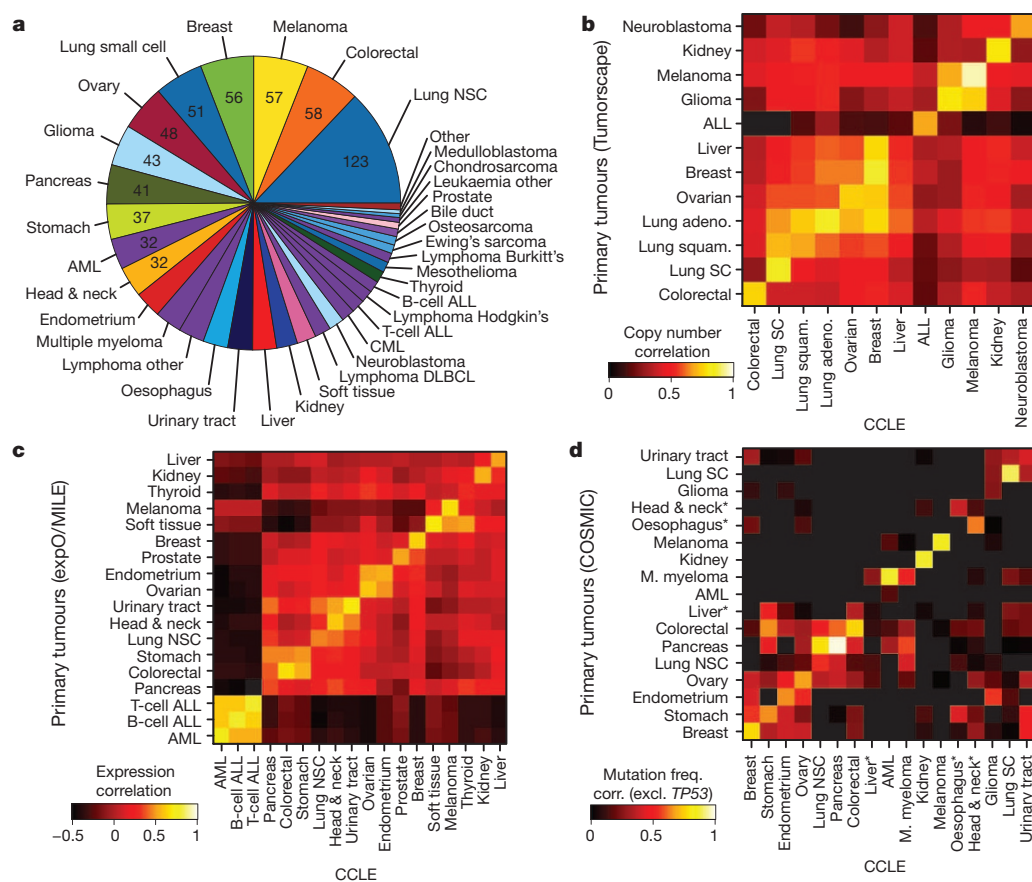*These authors contributed equally to this work.

Figure 1 | The Cancer Cell Line Encyclopedia. a, Distribution of cancer types in the CCLE by lineage. b, Comparison of DNA copy-number profiles (GISTIC G-scores) between cell lines and primary tumours. The diagonal of the heat map shows the Pearson correlation between corresponding tumour types. Because cell lines and tumours are separate data sets, the correlation matrix is asymmetric: the top left showing how well the tumour features correlate with the average of the cell lines in a lineage, and the bottom right showing the converse. c, Comparison of mRNA expression profiles between cell lines and primary tumours. For each tumour type, the log fold change of the 5,000 most variable genes is calculated between that tumour type and all others. Pearson correlations between tumour type fold changes from primary tumours and cell lines are shown as a heat map. d, Comparison of point mutation frequencies between cell lines and primary tumours in COSMIC (v56), restricted to genes that are well represented in both sample sets but excluding TP53, which is highly prevalent in most tumour types. Pairwise Pearson correlations are shown as a heat map. Asterisk indicates that the correlations of oesophageal, liver, and head and neck cancer mutation frequencies are restored when including TP53.

PLX4720, with sensitive lines enriched for the $BRAF^{V600E}$ mutation (Fig. 2a). To capture simultaneously the efficacy and potency of a drug, we designated an 'activity area' (Fig. 2b and Supplementary Fig. 6). The 24 compounds profiled showed wide variations in activity area, and those with similar mechanisms of action clustered together (Supplementary Fig. 7).

Genomic correlates of drug sensitivity may be extracted by predictive models using machine learning techniques[6,10]. We therefore assembled all CCLE genomic data types into a matrix wherein each feature was converted to a z-score across all lines (Supplementary Methods). Next, we adapted a categorical modelling approach that used a naive Bayes classification and discrete sensitivity calls, or an elastic net regression analysis[16] for continuous sensitivity measurements. Both approaches were applied to all compounds and genomic data with or without gene expression features (Supplementary Methods). Prediction performance was determined using tenfold cross-validation, and the elastic net features were bootstrapped to retain only those that were consistent across runs (Supplementary Methods).

Out of >50,000 input features, the regression-based analysis identified multiple known features as top predictors of sensitivity to several agents (Supplementary Table 7 and Supplementary Figs 8 and 9), with robust cross-validated performance (Supplementary Fig. 10 and 11). For example, activating mutations in BRAF and NRAS were among the top four predictors of sensitivity in models generated for the MEK inhibitor PD-0325901 (ref. 10) (Fig. 2c). Additional predictive features for MEK inhibition included expression of PTEN, PTPN5 and SPRY2 (which encodes a regulator of MAPK output). KRAS mutations were also identified, albeit with a lower predictive value (Fig. 2c, Supplementary Tables 8 and 9 and Supplementary Fig. 8).

Other top predictors included EGFR mutations and ERBB2 amplification/overexpression for erlotinib[8] and lapatinib[17], respectively;

$BRAF^{V600E}$ for RAF inhibitors (PLX4720 (ref. 18) and RAF265); HGF expression and MET amplification for the MET/ALK inhibitor PF-2341066 (ref. 19); and MDM2 overexpression for Nutlin-3 (ref. 20) sensitivity. Variants affecting the EXT2 gene, which encodes a glycosyltransferase involved in heparin sulphate biosynthesis, were significantly correlated with erlotinib effects (Supplementary Fig. 12). This observation is intriguing in light of a report linking heparin sulphate with erlotinib sensitivity[21]. In addition, NQO1 expression was identified as the top predictive feature for sensitivity to the Hsp90 inhibitor 17-AAG, a quinone moiety metabolized by NAD(P)H:quinone oxidoreductase (NQO1). NQO1 produces a high-potency intermediate (17-AAGH2)[22], and has previously been identified as a potential biomarker for Hsp90 inhibitors[23].

Because some genetic/molecular alterations occur commonly in specific tumour types, lineage may become a confounding factor in predictive analyses. Indeed, a classifier built using the entire cell-line data set performed suboptimally when applied exclusively to melanoma-derived cell lines (Fig. 2d), whereas a model built with only melanoma cell lines performed better (Fig. 2d). Predictive features in the melanoma-only model showed a strong overexpression of genes regulated by the transcription factors MITF and SOX10 (Supplementary Table 10), which may also help predict RAF inhibitor drug sensitivity in melanoma cell lines.

Nonetheless, lineage emerged as the predominant predictive feature for several compounds. For example, elastic net studies of the HDAC inhibitor panobinostat identified haematological lineages as predictors of sensitivity (Fig. 2e and Supplementary Fig. 9). Interestingly, most clinical responses to panobinostat and related compounds (for example, vorinostat and romidepsin) have been observed in haematological cancers. Similarly, most multiple myeloma cell lines (12 of 14 lines tested) exhibited enhanced sensitivity to the IGF1 receptor inhibitor
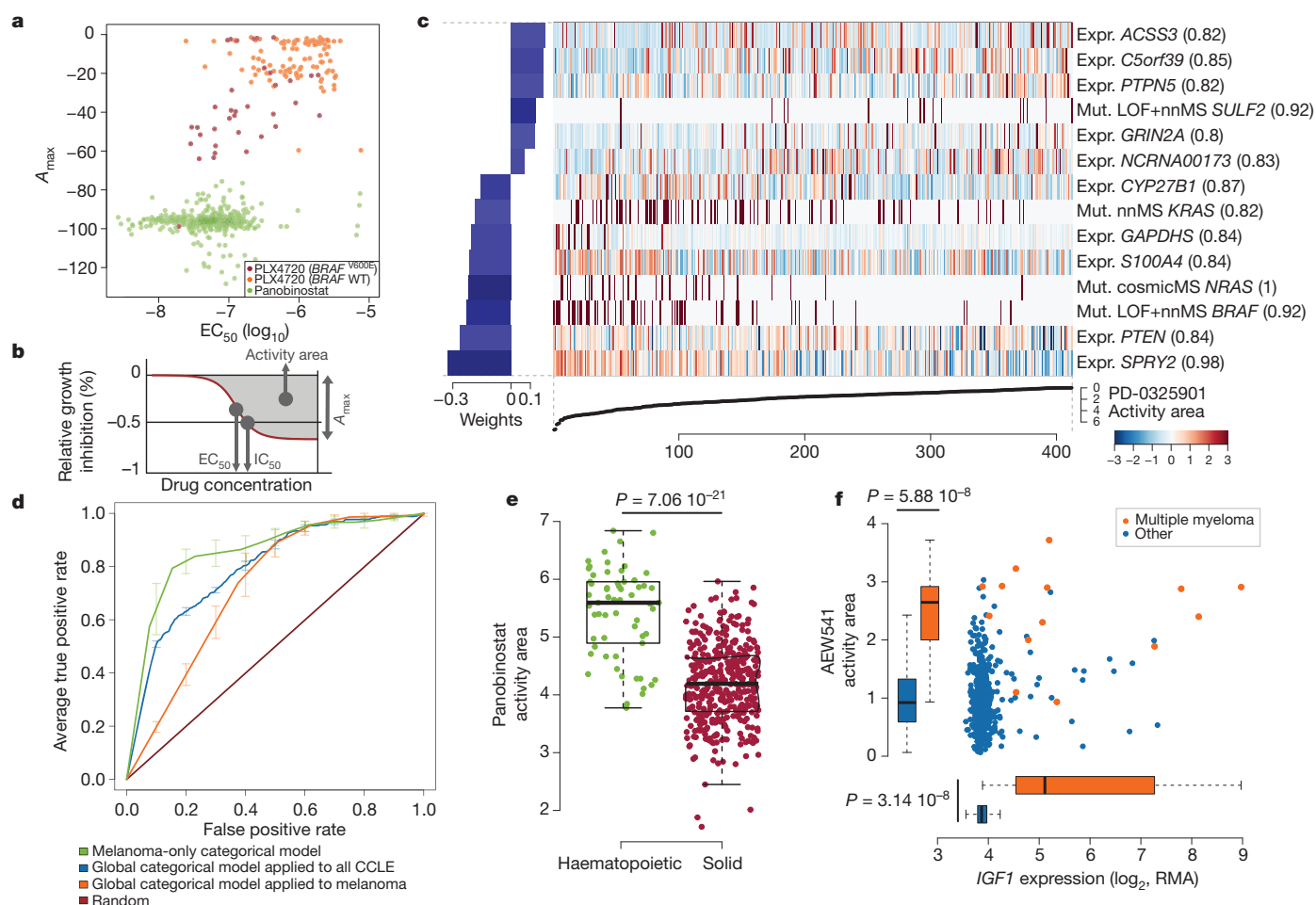
Figure 2 | Predictive modelling of pharmacological sensitivity using CCLE genomic data. a, b, Drug responses for panobinostat (green) and PLX4720 (orange/purple) represented by the high-concentration effect level (A_{max}) and transitional concentration (EC_{50}) for a sigmoidal fit to the response curve (**b**). **c,** Elastic net regression modelling of genomic features that predict sensitivity to PD-0325901. The bottom curve indicates drug response, measured as the area over the dose–response curve (activity area), for each cell line. The central heat map shows the CCLE features in the model (continuous *z*-score for expression and copy number, dark red for discrete mutation calls), across all cell lines (*x* axis). Bar plot (left): weight of the top predictive features for sensitivity (bottom) or insensitivity (top). Parentheses indicate features present in >80% of models after bootstrapping. LOF, loss of function mutation; nnMS, non-neutral missense mutation (Supplementary Methods).

d, Specificity and sensitivity (receiver operating characteristic curves) of cross-validated categorical models predicting the response to a MEK inhibitor, PD-0325901 (activity area). Mean true positive rate and standard deviation ($n = 5$) are shown when models are built using all lines (global categorical model, in blue and orange), or within only melanoma lines (green). **e,** Activity area values for panobinostat between cell lines derived from haematopoietic ($n = 61$) and solid tumours ($n = 387$). The middle bar, median; box, inter-quartile range; bars extend to 1.5× the inter-quartile range. **f,** Distribution of activity area values for AEW541 relative to *IGF1* mRNA expression. Orange dots, multiple myeloma cell lines ($n = 14$); blue dots, cell lines from other tumour types ($n = 434$). Box-and-whisker plots show the activity area or mRNA expression distributions relative to each cell line type (line, median; box, inter-quartile range), with bars extending to 1.5× the inter-quartile range.

AEW541 (Fig. 2f and Supplementary Figs 8 and 9) and showed high *IGF1* expression (Fig. 2f). Interestingly, elevated *IGF1R* expression also correlated with AEW541 sensitivity (Supplementary Fig. 9). The CCLE results indicate that multiple myeloma may be a promising indication for clinical trials of IGF1 receptor inhibitors[24] and that these drugs may have enhanced efficacy in cancers with high *IGF1* or *IGF1R* expression.

Whereas *BRAF* and *NRAS* mutations are known single-gene predictors of sensitivity to MEK inhibitors, several 'sensitive' cell lines lacked mutations in these genes, whereas other lines harbouring these mutations were nonetheless 'insensitive' (Fig. 2c). The elastic net regression model derived from the subset of cell lines with validated *NRAS* mutations identified elevated expression of the *AHR* gene (which encodes the aryl hydrocarbon receptor) as strongly correlated with sensitivity to the MEK inhibitor PD-0325901 (Fig. 3a). This finding was interesting in light of previous studies indicating that a related MEK inhibitor (PD-98059) may also function as a direct AHR antagonist[25]. We therefore hypothesized that the enhanced sensitivity of some *NRAS*-mutant cell lines to MEK inhibitors might relate to a coexistent dependence on AHR function.

To test this hypothesis, we first confirmed the correlation between *AHR* expression and sensitivity to MEK inhibitors in a subset of *NRAS*-mutant cell lines (Fig. 3b and Supplementary Fig. 13). Next, we performed short hairpin RNA (shRNA) knockdown of *AHR* in cell lines with high or low AHR expression (Fig. 3c). Silencing of *AHR* suppressed the growth of three *NRAS*-mutant cell lines with elevated *AHR* expression (Fig. 3d–f), but had no effect on the growth of two lines with low AHR expression (Fig. 3g, h). The growth inhibitory effect was confirmed with two additional shRNAs, where evidence for dose dependence was also apparent (Fig. 3i, j). We also tested the hypothesis that allosteric MEK inhibitors may suppress AHR function by measuring the effect of PD-0325901 and PD-98059 on endogenous *CYP1A1* mRNA, a transcriptional target of AHR in some contexts. Both compounds reduced *CYP1A1* levels in *NRAS*-mutant melanoma cells (IPC-298 and SK-MEL-2; Fig. 3k) but not in neuroblastoma cells (CHP-212; Fig. 3k), indicating that other factors may govern *CYP1A1* expression in the latter lineage. Together, these results suggest that AHR dependency may co-occur with MAP kinase activation in some *NRAS*-mutant cancer cells, and that elevated AHR may serve as a
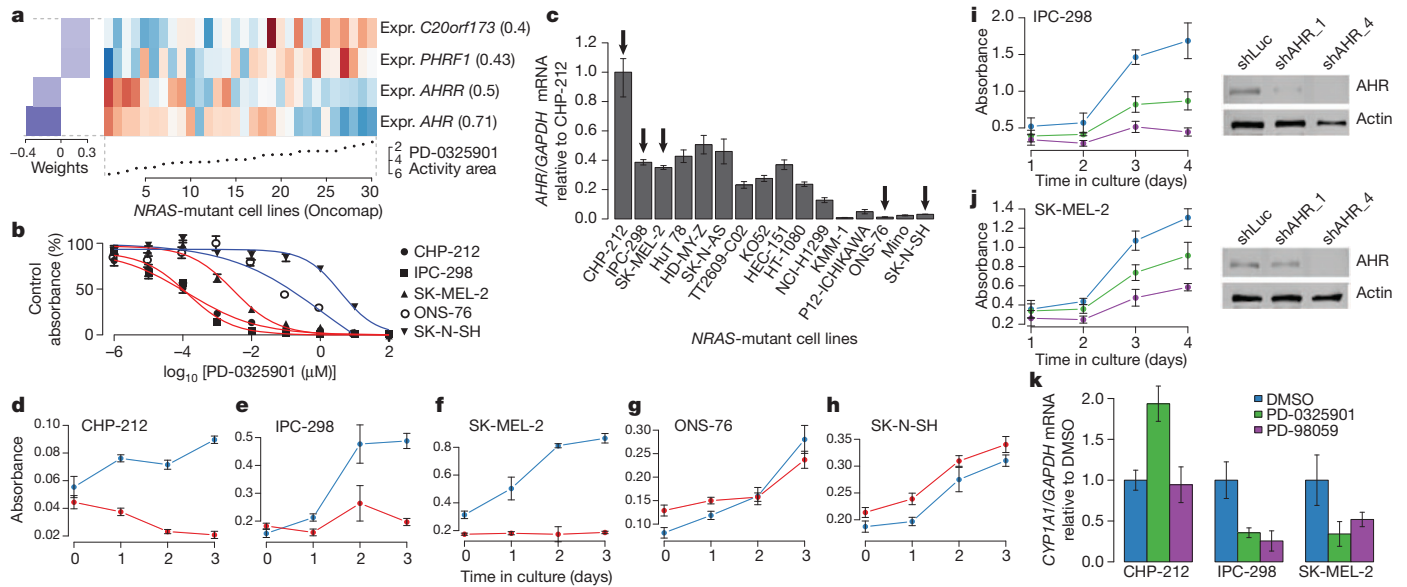
Figure 3 | *AHR* expression may denote a tumour dependency targeted by MEK inhibitors in *NRAS*-mutant cell lines. a, Predictive features for PD-0325901 sensitivity (using the 'varying baseline' activity area) in validated *NRAS*-mutant cell lines. **b**, Growth inhibition curves for *NRAS*-mutant cell lines expressing high (red) or low (blue) levels of *AHR* mRNA in the presence of the MEK inhibitor PD-0325901. **c**, Relative *AHR* mRNA expression across a panel of *NRAS*-mutant cell lines (arrows indicate cell lines where AHR dependency was analysed). **d–h**, Proliferation of *NRAS*-mutant cell lines displaying high (**d–f**) and low (**g**, **h**) *AHR* mRNA expression, after introduction of shRNAs against

AHR (red lines) or luciferase (blue lines). **i**, Left: proliferation of IPC-298 cells (high AHR) after introduction of additional shRNAs against *AHR* (shAHR_1 and shAHR_4; green and purple lines, respectively) or luciferase (control shLuc; blue line). Right: corresponding immunoblot analysis of AHR protein. **j**, Equivalent studies as in **i** using SK-MEL-2 cells (high AHR). **k**, Endogenous *CYP1A1* mRNA expression in the neuroblastoma line CHP-212 or the melanoma lines IPC-298 and SK-MEL-2 after exposure to vehicle (blue) or MEK inhibitors (PD-0325901, green or PD-98059, purple). Error bars indicate standard deviation between replicates, with *n* = 12 (**b**), *n* = 3 (**c**), *n* = 6 (**d–k**).

mechanistic biomarker for enhanced MEK inhibitor sensitivity in this setting.

We also looked for markers predictive of response to several conventional chemotherapeutic agents (Supplementary Fig. 7 and Supplementary Table 6) and identified *SLFN11* expression as the top correlate of sensitivity to irinotecan (Fig. 4a), a camptothecin analogue that inhibits the topoisomerase I (TOP1) enzyme. *SLFN11* expression
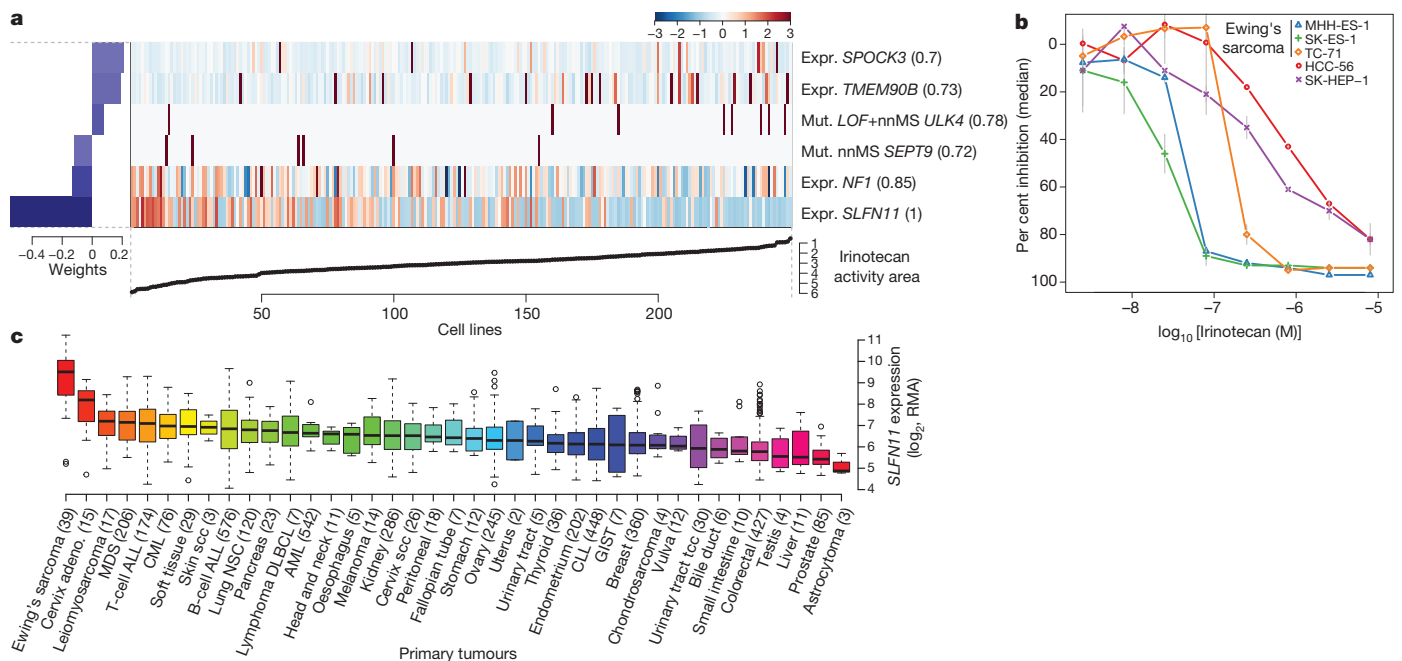
also emerged as the top predictor of topotecan sensitivity (another TOP1 inhibitor; Supplementary Figs 8 and 14). Overall, 12 of 16 lineages showed significant *SLFN11* associations for topotecan or irinotecan sensitivity (Pearson's $r \geq 0.2$, Supplementary Fig. 14b). This finding was independently validated using data from the NCI-60 collection (Supplementary Fig. 15). *SLFN11* knockdown did not affect steady-state growth sensitivity profiles (Supplementary Fig. 14d–f).

Figure 4 | Predicting sensitivity to topoisomerase I inhibitors. a, Elastic net regression analysis of genomic correlates of irinotecan sensitivity is shown for 250 cell lines. **b**, Dose–response curves for three Ewing's sarcoma cell lines (MSS-ES-1, SK-ES-1 and TC-71) and two control cell lines with low *SLFN11* expression (HCC-56 and SK-HEP-1). Grey vertical bars, standard deviation of

the mean growth inhibition (*n* = 2). **c**, *SLFN11* expression across 4,103 primary tumours. Box-and-whisker plots show the distribution of mRNA expression for each subtype, ordered by the median *SLFN11* expression level (line), the inter-quartile range (box) and up to 1.5× the inter-quartile range (bars). Sample numbers (*n*) are indicated in parentheses.

All three Ewing's sarcoma cell lines screened showed both high *SLFN11* expression and sensitivity to irinotecan (Fig. 4b and Supplementary Fig. 14). Ewing's sarcomas also exhibited the highest *SLFN11* expression among 4,103 primary tumour samples spanning 39 lineages (Fig. 4c), suggesting that TOP1 inhibitors might offer an effective treatment option for this cancer type. Towards this end, several ongoing trials in Ewing's sarcoma are examining irinotecan-based combinations, or the addition of topotecan to standard regimens[26]. For some lineages with high *SLFN11* expression (for example, cervical adenocarcinoma), topoisomerase inhibitors already comprise a standard chemotherapy regimen. In other tumours where topoisomerase inhibitors are commonly used (for example, colorectal and ovarian cancers), a range of *SLFN11* expression was observed, raising the possibility that high *SLFN11* expression might enrich for tumours more likely to respond. If confirmed in correlative clinical studies, *SLFN11* expression may offer a means to stratify patients for topoisomerase inhibitor treatment.

By assembling the CCLE, we have expanded the process of detailed annotation of preclinical human cancer models (http://www.broadinstitute.org/ccle). Genomic predictors of drug sensitivity revealed both known and novel candidate biomarkers of response. Even within genetically defined sub-populations—or when agents were broadly active without clear genetic targets—elastic net modelling studies identified key predictors or mechanistic effectors of drug response. Additional efforts that increase the scale and provide complementary types of information (for example, whole-genome/transcriptome sequencing, epigenetic studies, metabolic profiling or proteomic/phosphoproteomic analysis) should enable additional insights. In the future, comprehensive and tractable cell-line systems provided through this and other efforts[27] may facilitate numerous advances in cancer biology and drug discovery.

METHODS SUMMARY

A total of 947 independent cancer cell lines were profiled at the genomic level (data available at http://www.broadinstitute.org/ccle and Gene Expression Omnibus (GEO) using accession number GSE36139) and compound sensitivity data were obtained for 479 lines (Supplementary Table 11). Mutation information was obtained both by using massively parallel sequencing of >1,600 genes (Supplementary Table 12) and by mass spectrometric genotyping (OncoMap), which interrogated 492 mutations in 33 known oncogenes and tumour suppressors. Genotyping/copy number analysis was performed using Affymetrix Genome-Wide Human SNP Array 6.0 and expression analysis using the GeneChip Human Genome U133 Plus 2.0 Array. Eight-point dose–response curves were generated for 24 anticancer drugs using an automated compound-screening platform. Compound sensitivity data were used for two types of predictive models that used the naive Bayes classifier or the elastic net regression algorithm. The effects of *AHR* expression silencing on cell viability were assessed by stable expression of shRNA lentiviral vectors targeting either this gene or luciferase as control. The effect of compound treatment on *AHR* target gene expression was assessed by quantitative RT–PCR. A full description of the Methods is included in Supplementary Information.

1. Caponigro, G. & Sellers, W. R. Advances in the preclinical testing of cancer therapeutic hypotheses. *Nature Rev. Drug Discov.* **10,** 179–187 (2011).
2. MacConaill, L. E. & Garraway, L. A. Clinical implications of the cancer genome. *J. Clin. Oncol.* **28,** 5219–5228 (2010).
3. Lin, W. M. *et al.* Modeling genomic diversity and tumor dependency in malignant melanoma. *Cancer Res.* **68,** 664–673 (2008).
4. Neve, R. M. *et al.* A collection of breast cancer cell lines for the study of functionally distinct cancer subtypes. *Cancer Cell* **10,** 515–527 (2006).
5. Sos, M. L. *et al.* Predicting drug susceptibility of non-small cell lung cancers based on genetic lesions. *J. Clin. Invest.* **119,** 1727–1740 (2009).
6. Dry, J. R. *et al.* Transcriptional pathway signatures predict MEK addiction and response to selumetinib (AZD6244). *Cancer Res.* **70,** 2264–2273 (2010).
7. Garraway, L. A. *et al.* Integrative genomic analyses identify MITF as a lineage survival oncogene amplified in malignant melanoma. *Nature* **436,** 117–122 (2005).
8. Greshock, J. *et al.* Molecular target class is predictive of *in vitro* response profile. *Cancer Res.* **70,** 3677–3686 (2010).
9. McDermott, U. *et al.* Identification of genotype-correlated sensitivity to selective kinase inhibitors by using high-throughput tumor cell line profiling. *Proc. Natl Acad. Sci. USA* **104,** 19936–19941 (2007).
10. Solit, D. B. *et al.* BRAF mutation predicts sensitivity to MEK inhibition. *Nature* **439,** 358–362 (2006).
11. Staunton, J. E. *et al.* Chemosensitivity prediction by transcriptional profiling. *Proc. Natl Acad. Sci. USA* **98,** 10787–10792 (2001).
12. Weinstein, J. N. *et al.* An information-intensive approach to the molecular pharmacology of cancer. *Science* **275,** 343–349 (1997).
13. Thomas, R. K. *et al.* High-throughput oncogene mutation profiling in human cancer. *Nature Genet.* **39,** 347–351 (2007).
14. Beroukhim, R. *et al.* The landscape of somatic copy-number alteration across human cancers. *Nature* **463,** 899–905 (2010).
15. Ross, D. T. *et al.* Systematic variation in gene expression patterns in human cancer cell lines. *Nature Genet.* **24,** 227–235 (2000).
16. Zou, H. & Hastie, T. Regularization and variable selection via the elastic net. *J. R. Stat. Soc. B* **67,** 301–320 (2005).
17. Konecny, G. E. *et al.* Activity of the dual kinase inhibitor lapatinib (GW572016) against HER-2-overexpressing and trastuzumab-treated breast cancer cells. *Cancer Res.* **66,** 1630–1639 (2006).
18. Tsai, J. *et al.* Discovery of a selective inhibitor of oncogenic B-Raf kinase with potent antimelanoma activity. *Proc. Natl Acad. Sci. USA* **105,** 3041–3046 (2008).
19. Zou, H. Y. *et al.* An orally available small-molecule inhibitor of c-Met, PF-2341066, exhibits cytoreductive antitumor efficacy through antiproliferative and antiangiogenic mechanisms. *Cancer Res.* **67,** 4408–4417 (2007).
20. Müller, C. R. *et al.* Potential for treatment of liposarcomas with the MDM2 antagonist Nutlin-3A. *Int. J. Cancer* **121,** 199–205 (2007).
21. Nishio, M. *et al.* Serum heparan sulfate concentration is correlated with the failure of epidermal growth factor receptor tyrosine kinase inhibitor treatment in patients with lung adenocarcinoma. *J. Thorac. Oncol.* **6,** 1889–1894 (2011).
22. Guo, W. *et al.* Formation of 17-allylamino-demethoxygeldanamycin (17-AAG) hydroquinone by NAD(P)H:quinone oxidoreductase 1: role of 17-AAG hydroquinone in heat shock protein 90 inhibition. *Cancer Res.* **65,** 10006–10015 (2005).
23. Kelland, L. R., Sharp, S. Y., Rogers, P. M., Myers, T. G. & Workman, P. DT-Diaphorase expression and tumor cell sensitivity to 17-allylamino, 17-demethoxygeldanamycin, an inhibitor of heat shock protein 90. *J. Natl Cancer Inst.* **91,** 1940–1949 (1999).
24. Moreau, P. *et al.* Phase I study of the anti insulin-like growth factor 1 receptor (IGF-1R) monoclonal antibody, AVE1642, as single agent and in combination with bortezomib in patients with relapsed multiple myeloma. *Leukemia* **25,** 872–874 (2011).
25. Reiners, J. J. Jr, Lee, J. Y., Clift, R. E., Dudley, D. T. & Myrand, S. P. PD98059 is an equipotent antagonist of the aryl hydrocarbon receptor and inhibitor of mitogen-activated protein kinase kinase. *Mol. Pharmacol.* **53,** 438–445 (1998).
26. Wagner, L. M. *et al.* Temozolomide and intravenous irinotecan for treatment of advanced Ewing sarcoma. *Pediatr. Blood Cancer* **48,** 132–139 (2007).
27. Garnett, M. J. *et al.* Systematic identification of genomic markers of drug sensitivity in cancer cells. *Nature* http://dx.doi.org/10.1038/nature11005 (this issue).

Author Contributions For the work described herein, J.B. and G.C. were the lead research scientists; N.S., K.V. and A.M.M. were the lead computational biologists; M.P.M., W.R.S., R.S. and L.A.G. were the senior authors. J.B., G.C., S.K., P.M., J.M., J.T., A.S., N.L. and K.A. performed cell-line procural and processing; P.M. and K.A. performed or directed nucleic acid extraction and quality control; S.G., W.W. and S.B.G. performed or directed genomic data generation; C.J.W., F.A.M., E.B.-F., I.H.E., P.A., M.dS., K.J. and V.E.M. performed pharmacological data generation; N.S., K.V., G.V.K., A.R., M.F.B., J.C., G.K.Y., M.D.J., T.L., M.R. and G.G. contributed to software development; N.S., K.V., A.A.M., J.L., G.V.K., D.S., A.R., M.L., M.F.B., A.K., P.R., J.C., G.K.Y., J.Y., M.D.J., L.W., C.H., E.P., J.P.M., V.C. and M.P.M. performed computational biology and bioinformatics analysis; J.B., G.C., N.S., L.M., J.E.M., J.J.-V., M.P.M., W.R.S., R.S. and L.A.G. performed biological analysis and interpretation; N.S., K.V., A.A.M., J.L., A.R., M.L., L.M., A.K., J.J.-V., J.C., G.K.Y. and J.Y. prepared figures and tables for the main text and Supplementary Information; J.B., G.C., N.S., K.V., A.A.M., J.L., G.V.K., J.J.-V., M.P.M. and L.A.G. wrote and edited the main text and Supplementary Information; J.B., G.C., N.S., K.V., S.K., C.J.W., J.L., S.M., C.S., R.C.O., T.L., L.McC., W.W., M.R., N.L., S.B.G., K.A. and V.C. performed project management; J.P.M., V.E.M., B.L.W., J.P., M.W., P.F., J.L.H., M.M. and T.R.G. contributed project oversight and advisory roles; and M.P.M., W.R.S., R.S. and L.A.G. provided overall project leadership.

Author Information Data have been deposited in the Gene Expression Omnibus (GEO) using accession number GSE36139 and are also available at http://www.broadinstitute.org/ccle. Reprints and permissions information is available at www.nature.com/reprints. The authors declare competing financial interests: details accompany the full-text HTML version of the paper at www.nature.com/nature. Readers are welcome to comment on the online version of this article at www.nature.com/nature. Correspondence and requests for materials should be addressed to L.A.G. (Levi_Garraway@dfci.harvard.edu) or R.S. (robert.schlegel@novartis.com).

CORRECTIONS & AMENDMENTS

Addendum: The Cancer Cell Line Encyclopedia enables predictive modelling of anticancer drug sensitivity

Jordi Barretina, Giordano Caponigro, Nicolas Stransky,
Kavitha Venkatesan, Adam A. Margolin, Sungjoon Kim,
Christopher J. Wilson, Joseph Lehár, Gregory V. Kryukov,
Dmitriy Sonkin, Anupama Reddy, Manway Liu,
Lauren Murray, Michael F. Berger, John E. Monahan,
Paula Morais, Jodi Meltzer, Adam Korejwa,
Judit Jané-Valbuena, Felipa A. Mapa, Joseph Thibault,
Eva Bric-Furlong, Pichai Raman, Aaron Shipway,
Ingo H. Engels, Jill Cheng, Guoying K. Yu, Jianjun Yu,
Peter Aspesi Jr, Melanie de Silva, Kalpana Jagtap,
Michael D. Jones, Li Wang, Charles Hatton,
Emanuele Palescandolo, Supriya Gupta, Scott Mahan,
Carrie Sougnez, Robert C. Onofrio, Ted Liefeld,
Laura MacConaill, Wendy Winckler, Michael Reich, Nanxin Li,
Jill P. Mesirov, Stacey B. Gabriel, Gad Getz, Kristin Ardlie,
Vivien Chan, Vic E. Myer, Barbara L. Weber, Jeff Porter,
Markus Warmuth, Peter Finan, Jennifer L. Harris,
Matthew Meyerson, Todd R. Golub, Michael P. Morrissey,
William R. Sellers, Robert Schlegel & Levi A. Garraway

In the Supplementary Information of this Letter, the use of distinct data normalization and directionality methods for pharmacological response calculations caused minor inconsistencies. We have therefore updated Supplementary Table 11 and some of the Supplementary Figures to resolve any confusion (see the Supplementary Information to this Addendum). We also wish to describe the relevant drug sensitivity normalization and response score calculations more completely.

Two versions of the drug response data were generated. First, raw activity values were calculated at each dose as $A = 100(T/U − 1)$, in which T represents the Cell Titer Glo (CTG) level measured for the compound-treated well, and U is the median level of the untreated wells across the plate. This raw A is 0% with no drug and 100% for fully active compounds, when no CTG is detected. Second, the data were adjusted to a plate surface pattern and normalized to the MG132 positive control, as described in the Supplementary Methods. This normalized A is also 0% with no drug, but 100% corresponds to the median MG132 response on that plate. Although normalized drug responses were used to determine EC_{50}, IC_{50} and A_{max} values, we used the raw drug responses for calculating the activity area (AA). This distinction is now clear in the corrected Supplementary Table 11 (the two AA measures, derived from raw or normalized data, correlate closely: $r = 0.98$).

The activity is the sum of differences between the measured A_i at concentration i and $A = 0$, excluding positive A values: $AA = \sum i\{0 − \min(0, A_i/100)\}$. This AA has a value of 0 with no drug, and $+8$ for a compound inhibiting at $A = 100\%$ at all eight drug concentrations, as illustrated in Fig. 2b of the original Letter. We hope that this definition eliminates any confusion that may have existed in the original Supplementary Methods (page 13) and enables others to reproduce our AA results starting from the raw drug sensitivity data. As a further means of clarification, we have added three columns to Supplementary Table 11 showing the raw (non-normalized) response data necessary to calculate AA, MG132 activity, and AA derived from normalized response data.

In addition, although all computational analyses used the above AA formula, a few Supplementary Figures (Supplementary Figs 6, 11, 9 and 14b) used a scale showing $8 − AA$. This value was used for display purposes, so that low values corresponded to sensitive cell lines and the visualization remained consistent with other sensitivity metrics (IC_{50}, A_{max}). This specification was noted in Supplementary Fig. 8 but had been inadvertently cut off the Supplementary Fig. 9 legend. We have therefore updated the Supplementary Fig. 9 legend to clarify where an inverted scale was used, and updated the scale of Supplementary Figs 6, 11 and 14b to reflect our definition of AA (noted above).

These changes do not affect the analyses, results or scientific conclusions presented in the paper. The authors are indebted to B. Yadav, who alerted them to these inconsistencies.

Supplementary Information is available in the online version of the Addendum.

CORRECTIONS & AMENDMENTS

Addendum: The Cancer Cell Line Encyclopedia enables predictive modelling of anticancer drug sensitivity

Jordi Barretina, Giordano Caponigro, Nicolas Stransky, Kavitha Venkatesan, Adam A. Margolin, Sungjoon Kim, Christopher J. Wilson, Joseph Lehár, Gregory V. Kryukov, Dmitriy Sonkin, Anupama Reddy, Manway Liu, Lauren Murray, Michael F. Berger, John E. Monahan, Paula Morais, Jodi Meltzer, Adam Korejwa, Judit Jané–Valbuena, Felipa A. Mapa, Joseph Thibault, Eva Bric–Furlong, Pichai Raman, Aaron Shipway, Ingo H. Engels, Jill Cheng, Guoying K. Yu, Jianjun Yu, Peter Aspesi Jr, Melanie de Silva, Kalpana Jagtap, Michael D. Jones, Li Wang, Charles Hatton, Emanuele Palescandolo, Supriya Gupta, Scott Mahan, Carrie Sougnez, Robert C. Onofrio, Ted Liefeld, Laura MacConaill, Wendy Winckler, Michael Reich, Nanxin Li, Jill P. Mesirov, Stacey B. Gabriel, Gad Getz, Kristin Ardlie, Vivien Chan, Vic E. Myer, Barbara L. Weber, Jeff Porter, Markus Warmuth, Peter Finan, Jennifer L. Harris, Matthew Meyerson, Todd R. Golub, Michael P. Morrissey, William R. Sellers, Robert Schlegel & Levi A. Garraway

Addendum to: *Nature* https://doi.org/10.1038/nature11003, published online 28 March 2012; addendum 28 November 2012.

The Supplementary Information of our original Letter (https://doi.org/10.1038/nature11003) and the Addendum published on 28 November 2012 (https://doi.org/10.1038/nature11735; hereafter referred to as 'first Addendum') contain all of the data used for our analyses. These data include normalized activity (growth inhibition) responses for every cell line at each dose for all 24 of the compounds and drugs tested. These activity values were calculated from replicated data points extracted from one or more experimental assay plates, and normalized using treated and untreated controls from the same plates; as detailed in the original Letter (see the original Supplementary Information 2, page 10), and in the first Addendum. In subsequent correspondence, readers expressed an interest in reproducing our experimental pre-processing, so we shared with them the raw Cell Titer Glo (CTG) data values from each experimental well. These data are now provided as a reference for future readers.

Supplementary Data 1 to this Addendum contains raw values from wells with cell lines growing under control (AC, positive active; NC, untreated negative) or drug-treated (SA, single-agent) conditions. Supplementary Data 1 contains two row entries per well (one with raw CTG readouts, and the other with calculated activity values), and each column contains descriptions or response values, as detailed in Table 1 of this Addendum. Only valid wells are included, so there may be missing concentrations from curves containing data that were flagged as 'invalid'. Compound and cell line names in Supplementary Data 1 are as they were originally captured, which in some cases may differ from names used in the Supplementary Tables of the original Letter and first Addendum. Calculated activity values may also differ in some cases from those in the original Letter, owing to subsequent quality-control call changes in our database since 2012. Chemical names can be reconciled using Table 2 of this Addendum, noting that 'sample-ID' denotes the 'ID-concept' of Table 2 with salt form and batch suffixes appended. Discrepant cell line names may be understood with reference to columns A, C and D of the 'All_Drug_response_data' sheet in supplementary data 1 from the 2015 CCLE and GDSC consortium paper[1].

1. The Cancer Cell Line Encyclopedia Consortium & The Genomics of Drug Sensitivity in Cancer Consortium. Pharmacogenomic agreement between two cancer cell line data sets. *Nature* **528**, 84–87 (2015).

Table 1 | Descriptions for key columns in Supplementary Data 1

Header	Description
CELL_LINE_NAME	Cell line name
MASTER_PLATE_NAME	Name of master plate for compound dispensing
PLATE_GROUP	Experimental batch identifier
ASSAY_PLATE_NAME	Barcode identifier for this experimental plate
DATE_CREATED	Date and time of experimental plate readout
LAYER_TYPE	CTG readout (RAW) or calculated activity (OUTPUT)
WELL_TYPE	Untreated (NC), positive (AC), or drug treated (SA)
COLUMN_ID	Column identifier for this experimental well
ROW_ID	Row identifier for this experimental well
COMPOUND	Sample-ID for the chemical used
CONCENTRATION	Compound concentration in micromoles
VALUE	Raw CTG readout value

CORRECTIONS & AMENDMENTS

Table 2 | Chemical name mappings

Name	ID-concept	Name-probe	Name-generic	Name-brand
paclitaxel	NVP-LEE850; NVP-BGT136; NVP-LLP829; CHIR167540	TL-139; BMS-181339; LSM-1102; MGI-GP; SW198621	paclitaxel	Taxol; Genexol; Abraxane
irinotecan	NVP-LBN777; CHIR169217	CPT-11; U-101440E; CPT11; LSM-2167; DQ-2805; NSC-616348; SW197790; SW199156	irinotecan	Camptosar; Campto; Topotecin
topotecan	NVP-LBN564; NVP-LBN816; CHIR158120; SN-38	SKF-104864; INOC-010; INX-0076; BRD-A36630025; 7-ethyl-10- hydroxycamptothecin; LSM-5662; E-89-001; NK-211; NSC-609699; SKF-S-104864-A; SW197557; SW199637	topotecan	Hycamtin; Evotropin; Topotecan; Hycamptin
panobinostat	NVP-LBH589	NVP-LBH589; LSM-4284; LBH-589	panobinostat	Faridak
L-685458	NVP-LLP590; NVP-AHK537; CGP055750	L-685458; L-682679; BRD-K87317732		
tanespimycin	NVP-LJM835; NVP-BAG500; NVP-LLP773; CHIR371658	17-AAG; CNF-1010; IPI-493; IPI-504; KOS-953; LSM-5870; BRD-K81473043; CP-127374; NSC-330507; NSC-704057	tanespimycin; retaspimycin; 17-allylaminogel-danamycin	
NVP-LBW242	NVP-LBW242; NVP-LDK934	CHEMBL1950720; SureCN2731929;NVP-LBW242; LBW242		
nutlin-3A	NVP-BEP453;	LSM-6351	nutlin-3A	
palbociclib	NVP-LCY393	PD-0332991; LSM-1071	palbociclib	
saracatinib	NVP-BHT496	AZD-0530; NSC-735464; KIN001-045; LSM-1032	saracatinib	
PLX-4720	NVP-LFL230; CHIR779209	PLX-4720; LSM-1049		
PD-0325901	NVP-LBW624; CHIR371086	PD-0325901; DB07046; CHEMBL447345; CHEMBL573579; CHEMBL573819; LSM-1101		
selumetinib	NVP-LFE158	AZD-6244; Arry-142886; LSM-1056; BRD-K57080016; ARRY-886	selumetinib	
NVP-RAF265	NVP-RAF265; HIR371265; HIR565852	CHIR-265; NVP-RAF265; LSM-1207		
nilotinib	NVP-AMN107; NVP-LOY196	NVP-AMN107; LSM-1099;AMN-107	nilotinib	Tasigna
NVP-TAE684	NVP-TAE684	NVP-TAE684; TAE-684; KIN001-017; LSM-1024		
crizotinib	NVP-LDQ718; NVP-BQK827	PF-2341066; KIN001-023; LSM-1027	crizotinib	Xalkori
erlotinib	NVP-XBX005; CHIR381147; CGP084057; CGP084057A	CP-258; OSI-774; RG-1415; Ro-50-8231; LSM-1097; CP-358774; NSC-718781; R-1415; SW198886	erlotinib	Tarceva
lapatinib	NVP-BCZ548	GW-2016; GW-572016F; GSK-572016; LSM-1051; W-572016; SW199101	lapatinib	Tykerb; Tyverb
dovitinib	NVP-TKI258; NVP-BAV666; CHIR154258	CHIR-258; TKI-258; NVP-TKI258; LSM-1127	dovitinib	
sandostatin	NVP-AES222; NVP-AEW541	NVP-AEW541; CC-535; LSM-1122; AEW541	sandostatin	
PHA-665752	NVP-BBD023	PHA-665752; SureCN140412; TCMDC-125885; LSM-1125		
vandetanib	NVP-AFD094; CHIR160840	ZD-6474; AZD-6474; LSM-1199	vandetanib	Caprelsa; Zactima
sorafenib	NVP-LBK294; CHIR156503	Bay-43-9006; NSC-724772; LSM-1008	sorafenib	Nexavar